Ceramics International 47 (2021) 23905–23918

Contents lists available at ScienceDirect

Ceramics International

journal homepage: www.elsevier.com/locate/ceramint

Effects of nanosilica and steel fibers on the impact resistance of slag based self-compacting alkali-activated concrete

Anıl Niş [a,*], Necip Altay Eren [b], Abdulkadir Çevik [b]

[a] Department of Civil Engineering, Istanbul Gelisim University, Istanbul, Turkey
[b] Department of Civil Engineering, Gaziantep University, Gaziantep, Turkey

ARTICLE INFO

Keywords:
Self-compacting alkali-activated concrete
Nanosilica
Steel fiber
Drop-weight test
Impact resistance
Impact energy

ABSTRACT

In this research, the effects of nanosilica and steel fibers on the impact resistance of ground granulated blast furnace slag based self-compacting alkali-activated concrete were investigated. Nanosilica volume fraction was kept constant at 2%. Two types of hooked-end steel fibers (Kemerix 30/40 and Dramix 60/80) and steel fiber volume contents (0.5% and 1%) were utilized to highlight the combined effects of nanosilica and steel fiber on the impact behavior. The fresh state and mechanical properties such as slump flow, L-box, V-funnel, compressive strength, modulus of elasticity, splitting tensile strength, and flexural strength were evaluated. The microstructure of the samples was examined using a scanning electron microscope. The impact resistance of the specimens was measured by a drop-weight test. Acceleration-time and force-time graphs were plotted and evaluated together with the crack photos of the specimens for the first and failure impactor drops. The incorporations of nanosilica and steel fiber improved splitting tensile strength, flexural strength, impact resistance, and energy absorption capacity, while they decreased compressive strength and modulus of elasticity. For the specimens without nanosilica and with 2% nanosilica, the impact energy improvements were five times and 12.5 times higher for 0.5% short fibrous, 20.5 times and 44.5 times higher for 1% short fibrous, 23.5 times and 31 times higher for 0.5% long fibrous, and 64 times and 144.5 times higher for 1% long fibrous specimens than the specimens without nanosilica and steel fiber, respectively. The long fibers were found more effective in mechanical strength and impact energy than short fibers, and the reinforcing efficiency of fibers enhanced with higher steel fiber volumes. The combined utilization of nanosilica and steel fibers have the potential to delay the crack formation and dissipate energy to the surrounding zones, and this potential increased with higher steel fiber lengths and volume ratios.

1. Introduction

Ordinary Portland cement (OPC) concrete is the second most utilized resource on earth after water, and OPC production contributes about 8% of all greenhouse gases released worldwide [1]. The need for OPC concrete will increase in the upcoming years due to the increasing population, natural disasters, i.e., earthquakes, storms, hurricanes. Also, Covid-19 and similar pandemics will cause high demand to the novel structural buildings for better-isolated areas. These reasons will continue to increase the amount of carbon dioxide released into the atmosphere. Researchers have made efforts to find alternative binders or construction materials to decrease the carbon dioxide burden on the planet [2]. Recently, geopolymer or alkali-activated concrete has emerged as an environment-friendly concrete as an alternative to OPC concrete, and it has a similar mechanical strength and durability performance with OPC concrete [3–5]. Alkali-activated concrete takes great attention due to the significant reduction in carbon dioxide release and the requirement of natural resources. Alkali-activated concrete can reduce the carbon dioxide footprint of OPC production by 80% when designed and appropriately produced with supplementary cementitious materials [2].

Geopolymer is considered as a clinker-free and low carbon binder [6], which composes of aluminosilicate including solids such as ground granulated blast furnace slag and fly ash [7,8] with alkali activators such as alkali sulfate, carbonate, silicate, and hydroxide [9]. Also, calcium (Ca) compounds play a significant role since calcium ions can act as a charge balancing cation in the geopolymer binder [10,11]. The geopolimerization process is a complex chemical process, and researchers

* Corresponding author.
E-mail address: anis@gelisim.edu.tr (A. Niş).

https://doi.org/10.1016/j.ceramint.2021.05.099
Received 4 March 2021; Received in revised form 9 May 2021; Accepted 12 May 2021
Available online 15 May 2021

Table 1
Chemical and physical characteristic of NS and GGBFS.

Component	CaO	SiO_2	Al_2O_3	Fe_2O_3	MgO	SO_3	K_2O	Na_2O	LOI	SG	BF (m^2/kg)
NS (%)	-	99.8	-	-	-	-	-	-	<1.00	2.20	-
GGBFS (%)	34.12	36.40	11.39	1.69	10.30	0.49	3.63	0.35	1.64	2.79	418

are trying to understand the influential parameters on the resulting mechanical and durability performance. It was reported that alumino-silicate composition, curing type and duration, alkali activator type and concentrations influence the resulting mechanical and durability performance [2,12]. Especially, fly ash based geopolymer concretes required elevated temperature curing, and for the complete dissolution of fly ash particles in the geopolimerization, the oven-curing should be higher than 40 °C [13] and 60 °C [14]. In a study, 13 different curing methods on the mechanical strength performance of fly ash and slag based geopolymer concretes were investigated. It was reported that oven-curing and delayed oven-curing (oven-curing applied later) also significantly enhanced the mechanical performance of fly ash based geopolymer concretes, while slag based alkali-activated concretes can be utilized in structural applications without oven-curing, delayed oven-curing, and water-curing [15]. Due to the lack of necessity of different curing regimes, slag based alkali-activated concretes were utilized in this study for the standardization process of alkali-activated concretes in structural applications.

Alkali-activated concrete, due to its brittle nature, similar to OPC concrete, exhibits insufficient toughness and deformation capacity, which pose enormous limitations for engineering applications. Thus, it is significant to improve the crack resistance and toughness of alkali-activated concrete [16]. To prevent the brittle behavior, various fiber types can be adding to alkali-activated concretes [17]. Despite there are different fiber types, steel fibers are still the most useable type [18]. The incorporation of steel fibers into the slag based alkali-activated concretes has contradictory results on the compressive strength performance. Some studies reported that steel fibers improve the compressive strength [19,20], while others confirmed an adverse effect on the resulting strength performance [21,22]. These results confirmed that additional research is required to obtain clear decisions. Meanwhile, in a comprehensive review study, it was reported that steel fibers favorably affect splitting tensile strength, flexural strength, toughness, ductility, crack propagation, and post-cracking; however, they have a negative effect on porosity and workability [18].

One way to eliminate the workability problem in steel fibrous concretes is to use self-compacting concrete (SCC) since SCC consolidates under its weight without vibration. It offers excellent workability and segregation resistance in addition to better mechanical and durability performances [23,24]. Also, the optimum steel fiber volume ratio was 1% due to the improved fiber orientation, flowability, and passing ability characteristics of SCC [25,26]. Thus, steel fiber volume was selected as 1% in the study.

Nowadays, researchers focus on utilizing nanosilica material in the concrete industry [27–29]. Nanosilica utilization generally enhances the mechanical performance and durability of concretes, which may be attributed to several mechanisms. Nanosilica is a very active pozzolan; therefore, it could improve concrete properties through the creation and tortuous microstructure. Also, nanosilica has a finer material, which could fill the ultrafine pores in the microstructure, leading to higher packing densities [30]. Thus, the utilization of nanosilica reduced the permeability and enhanced the mechanical and durability properties of concrete [27,28,31]. However, the effect of nanosilica on the mechanical performance of slag based self-compacting alkali-activated concrete is limited in the literature. In addition, the combined influence of steel fibers and nanosilica on the mechanical performance of self-compacting slag based alkali-activated concrete is very rare. Therefore, one of the aims was to study the combined effect of steel fibers and nanosilica on the mechanical performance of self-compacting alkali-activated concrete.

Recently, structural buildings have been exposed to impacts loads such as vehicular crashes, collisions due to earthquakes/hurricanes, or terror attacks [32]. Therefore, structures have to resist impact loadings in addition to axial and shear forces, and moments resulting from both vertical (weight of the structure) and horizontal (earthquake and wind) loadings. During impact loadings, a structure must absorb a large amount of energy suddenly. Therefore, high energy absorption capacity and ductility of structures are significant requirements under impact loadings.

Some previous investigations evaluated the impact performance of SCC reinforced with steel fibers. In a recent study, the impact resistance of steel fiber reinforced SCC was investigated by 0.5%, 0.75%, and 1% fiber volumes. It was reported that impact resistance increased with an increase in steel fiber volume, and the highest impact resistance was obtained on the SCC reinforced with a 1% fiber volume. The authors also stated that steel fiber content is suggested to be no more than 1% to obtain adequate passing ability characteristics of SCC [33]. In another research, the number of blows at first crack and failure stages were studied on self-compacting concrete reinforced with 0.5%, 0.75%, and 1% micro steel fibers. The authors found that the number of blows at first crack and failure increased with the increase of steel fiber content [34]. The impact resistance of OPC concrete with/out steel fibers was widely investigated in the literature. However, the influences of nanosilica and steel fibers on the impact performance of slag based self-compacting alkali-activated concrete have not been studied yet. For the first time, the detailed impact resistance of the self-compacting alkali activated concrete with/out nanosilica and steel fiber was investigated in this research.

2. Experimental procedure

2.1. Materials

The industrial waste material, ground granulated blast furnace slag (GGBFS) was used as a binder to produce the self-compacting alkali activated concrete (SCAAC) mixes. GGBFS with a specific surface area and a specific gravity of 418 m^2/kg and 2.79 respectively, was utilized in the study. Also, nanosilica (NS) was incorporated in a colloidal form into some of the mixes to evaluate the influence of NS on the resulting impact and fundamental mechanical performance. The specific surface and specific gravity of NS material were 150,000 kg/m^2 and 2.2 g/cm^3. The NS amount was utilized as 2% by weight of the GGBFS material and its particle size was in the range of 5–14 nm. Table 1 shows the chemical compositions and physical characteristics of NS and GGBFS materials.

Table 2
The sieve analysis and physical properties of aggregates.

Sieve Size (mm)	16	8	4	2	1	0.5	0.25	Fineness Modules	Specific Gravity	Absorption (%)
Fine Aggregate	100	100	100	67.3	39.9	28.4	16.4	2.57	2.45	1.5
Coarse Aggregate	100	31.5	1	0.5	0.5	0.5	0.4	5.66	2.72	2.4

Table 3
Component of SCAAC mixes.

Sample	GGBFS	NS	SF	Fine Agg.	Coarse Agg.	Na_2SO_3 +NaOH	Molarity	SP	Ekstra Water
	kg/m^3	kg/m^3	kg/m^3	kg/m^3	kg/m^3	kg/m^3		%	%
GB	500	0	0	860.07	738.12	250	12	7	10
GB-SF1/0.5	500	0	39.2	860.07	738.12	250	12	7	10
GB-SF1/1.0	500	0	78.4	860.07	738.12	250	12	7	10
GB-SF2/0.5	500	0	39.2	860.07	738.12	250	12	7	10
GB-SF2/1.0	500	0	78.4	860.07	738.12	250	12	7	10
GBN	490	10	0	858.49	736.76	250	12	7	10
GBN-SF1/0.5	490	10	39.2	858.49	736.76	250	12	7	10
GBN-SF1/1.0	490	10	78.4	858.49	736.76	250	12	7	10
GBN-SF2/0.5	490	10	39.2	858.49	736.76	250	12	7	10
GBN-SF2/1.0	490	10	78.4	858.49	736.76	250	12	7	10

The crushed limestone coarse and fine aggregates were achieved from the source utilized to obtain SCAAC mixes. Both the fine and coarse aggregates met the requirements of the aggregate grading curve conforming to the region of A-B in the TS802 standard, which corresponds to the area of well-graded aggregate. Table 2 illustrates the physical properties and the sieve analysis of the used aggregates. Sodium hydroxide (solid form as pellets 97%–98% purity) and sodium silicate (SiO_2: 29.4, water: 55.9%, and Na_2O: 13.7% by mass) mixture was utilized as an alkali activator. In an earlier investigation, the sodium silicate to sodium hydroxide ratio was suggested to be between 1.5 and 2.5 for economic reasons [35]; therefore, this ratio was selected as 2.5 in the research. The sodium hydroxide molarity was selected as 12 M, which showed the best mechanical performance for SCAAC [36].

In the previous investigation, three steel fiber shapes; hooked-end, corrugated, and straight steel fibers, were examined, and hooked-end steel fibers performed the best mechanical performance [37]. Therefore, hooked-end steel fibers, Kemerix 30/40 and Dramix 60/80 were utilized in this study. The Kemerix 30/40 hooked-end steel fibers (notated as SF1), having a length of 30 mm, an aspect ratio of 40, and a diameter of 0.75 mm, and the Dramix 60/80 hooked-end steel fibers (notated as SF2), having a length of 60 mm, an aspect ratio of 80, and a diameter of 0.75 mm, were utilized at fiber volume ratios of 0.5%, and 1%. Also, a polycarboxylate-ether-based MasterGlenium-RMC-303 superplasticizer was used to satisfy the SCC requirements.

2.2. Mix-design

Table 3 illustrates the mix ingredients of the SCAAC specimens. GB shows the SCAAC without NS and SF, GBN indicates the SCAAC with 2% NS and without SF, 0.5% and 1% refers to steel fiber volume ratios, and SF1 and SF2 demonstrate the Kemerix 30/40 and Dramix 60/80 hooked-end steel fibers, respectively. GGBFS amount was selected as 500 kg/m^3,

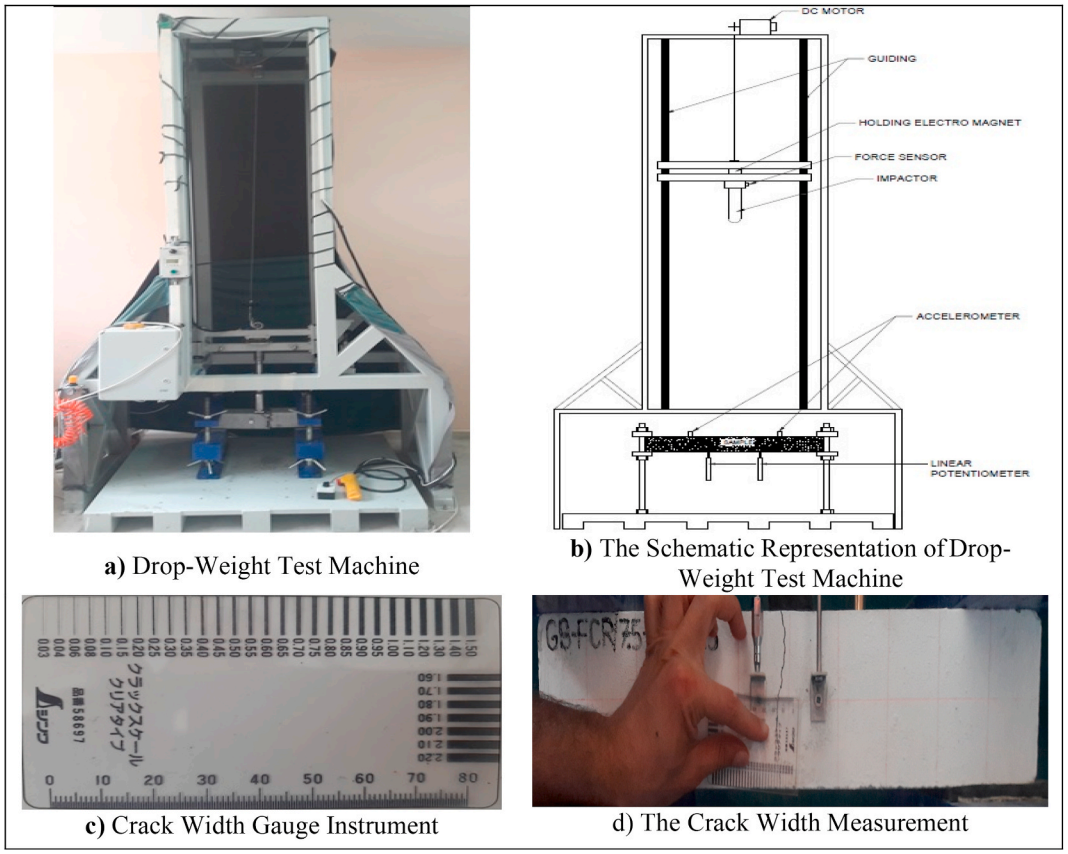

Fig. 1. Drop-weight impact test set-up.

and NS was used to replace GGBFS by 2%. A polycarboxylate-ether-based SP was incorporated into the SCAAC mixes by 7% weight of GGBFS to obtain the required workability and passing ability. For the workability improvement and further alkali activation, additional water utilization into the mixes was also reported in the previous investigations [38]. Thus, extra water was also added in this study to produce reasonably cheaper SCAAC production.

During the mixing period, aggregates and binder were firstly mixed in a dry state for 2.5 min. The SP, extra water, and alkali activator were included in 1 min to the dry mix and mixed for 2 min. Subsequently, the mixture was further mixed for extra 3 min to confirm the uniformity and homogeneity of SCAAC mixes. Then, fresh state tests were executed for each different concrete type. Then, the mixtures were cast into 100 × 100 × 500 mm beam sections for the drop-weight impact and flexural strength, 100 × 100 × 100 mm cubic sections for the compressive strength, and 100 × 200 mm cylinder sections for the splitting tensile strength and elasticity modulus tests. After the sample casting process, the top surfaces of the samples were covered with a sheet to eliminate the evaporation of alkali activators. The specimens were demolded and left in the laboratory environment at 23 ± 2 °C for 28 days.

2.3. Fresh state tests

The fresh state tests of the SCAAC mixtures were conducted using V-funnel, slump flow, and L-Box tests. The slump flow and V-funnel tests were executed to assess the flowability and viscosity requirements, and L-box tests were conducted to evaluate passing ability. The detailed fresh state tests procedure was explained in the previous studies. The flowability and viscosity of the mixes were measured using slump flow and V-funnel tests, and passing ability was measured by L-Box tests. The detailed test procedures of the slump flow, V-funnel, and L-box tests were explained in detail in the earlier investigation [26,31].

2.4. Hardened state tests

The 100 × 100 × 100 mm cube SCAAC specimens were used to obtain compressive strength values according to the ASTM C39 standard. The 100 × 200 mm cylinder samples were utilized in the elasticity modulus and splitting tensile strength tests executed by ASTM C496 standard. The four-point flexural strength tests were realized on 100 × 100 × 500 mm SCAAC beam samples under displacement-controlled loading with a rate of 0.02 mm/min. In addition, drop-weight impact tests were also realized by ACI Committee 544 recommendations, and the impact tests were realized in the form of repeated impacts to the same spot. A drop hammer periodically impacted to the middle part of a prismatic beam sample at a certain drop height and position. Fig. 1 shows the schematic representation of the drop-weight test machine and cracks width measurements.

For this purpose, the beam specimens of 100 × 100 × 500 mm were executed to study the impact resistance. An impactor weight of 28.5 kg was allowed to free fall from 10 cm height on the middle part of beam specimens. During impact tests, force-time, acceleration-time, displacement-time, and crack propagation data were collected simultaneously using a load cell to obtain the force, two potentiometers to measure vertical displacements, two accelerometers to measure accelerations during vibrations, and crack width gauge instruments to measure crack widths for each number of blows. The number of blows to cause the failure was used to obtain the failure impact energy by the following equation:

$$E_{impact} = m \times g \times h \times N$$

where, E_{impact}: impact energy in Joule (J); m: mass of the drop hammer = 28.5 kg; g: 9.81 m/s^2; h: releasing height of drop hammer (10 cm); N: number of blows.

In literature, there is no existing standard for the flexural impact tests. Zhang et al. listed different drop weights and drop heights used in the impact tests, and they reported that the changes of weight and drop height have a significant influence on the impact performance, although the failure modes are very different. They pointed out that the drop weight and drop height should be carefully considered when the researchers design the equipment of impact test and carry out the impact tests [39]. In this research, drop height was determined after preliminary experiments for specimens without steel fibers and nanosilica. As a result, 10 cm height was chosen as the weakest specimen failed after 2 drops, and it was the minimum height to obtain sensitive drop numbers regarding the specimens. In the impact machine, a special mechanism was constructed to prevent rebound after each impact. This mechanism has photocell sensors which initiate an air compressor mechanism that catches the impactor after the first drop and prevents the rebound of the impactor. The first cracking case of the specimens can be determined when a sudden change or overload sign was observed on the strains, indicating the formation of visible cracks i.e. 0.1 mm at the specimen surface. The failure of the specimens occurs after the breaking of the bond between steel fibers and matrix, resulting in the separation of beam specimens into two halves.

Table 4
The fresh state properties of SCAAC mixes.

Sample	S-Flow (mm)	L-Box (PL)	V-Funnel (s)	T_{50} (s)
GB	741	1	10.71	2.46
GB-SF1/0.5	707	0.96	14.25	3.13
GB-SF1/1.0	664	0.83	19.91	3.63
GB-SF2/0.5	693	0.94	17.09	3.37
GB-SF2/1.0	659	0.81	23.49	4.07
GBN	750	1	9.25	2.21
GBN-SF1/0.5	720	0.97	13.88	2.87
GBN-SF1/1.0	687	0.85	18.33	3.59
GBN-SF2/0.5	710	0.96	16.62	3.23
GBN-SF2/1.0	661	0.82	22.61	3.97

3. Result and discussions

3.1. Fresh state properties

Table 4 presents flowability and passing ability characteristics of the SCAAC mixes. The minimum flowability of the GB-SF2/1.0 mix was measured as 659 mm, which is above the minimum flow values of 550 mm and 600 mm according to EFNARC specification and EN 12350-8 standard, respectively. For the V-funnel tests, the discharge time of the V-funnel section should be a maximum of 15s to obtain excellent filling performance by EN 12350-9 standard. The results showed that only 1% steel fiber incorporating mixes were found above the 15s. However, no blocking was observed, and the other mixed satisfied the 15s criterion, indicating excellent filling ability for non-fibrous and 0.5% steel fibrous mixes. The EN 12350-9 standard indicated that T50 duration should be above 6s for high flowability, and all mixes satisfied this condition. In the L-box test, all PL values of the SCAAC mixes were above the minimum PL value criterion of 0.8 according to EN 12350-10 standard, resulting in an adequate passing ability of all SCAAC mixes. The results pointed out that all SCAAC mixes had adequate flowability and passing ability characteristics. The fresh state results also revealed that NS incorporations slightly enhanced both flowability and passing ability characteristics of SCAAC mixes. At the same time, steel fiber inclusions reduced both flowability and passing ability, and the reduction was more with an increased steel fiber aspect and volume ratios.

It is known that every SCC should possess three features; flowability, passing ability, and segregation resistance. The first two fresh properties were tested in this study, the third was not, which is usually tested using the ASTM rapid penetration resistance test. Segregation resistance becomes significant with higher flowability (especially for 760 mm or more - SF3 class) and lower viscosity (VF1 category). In this study, all

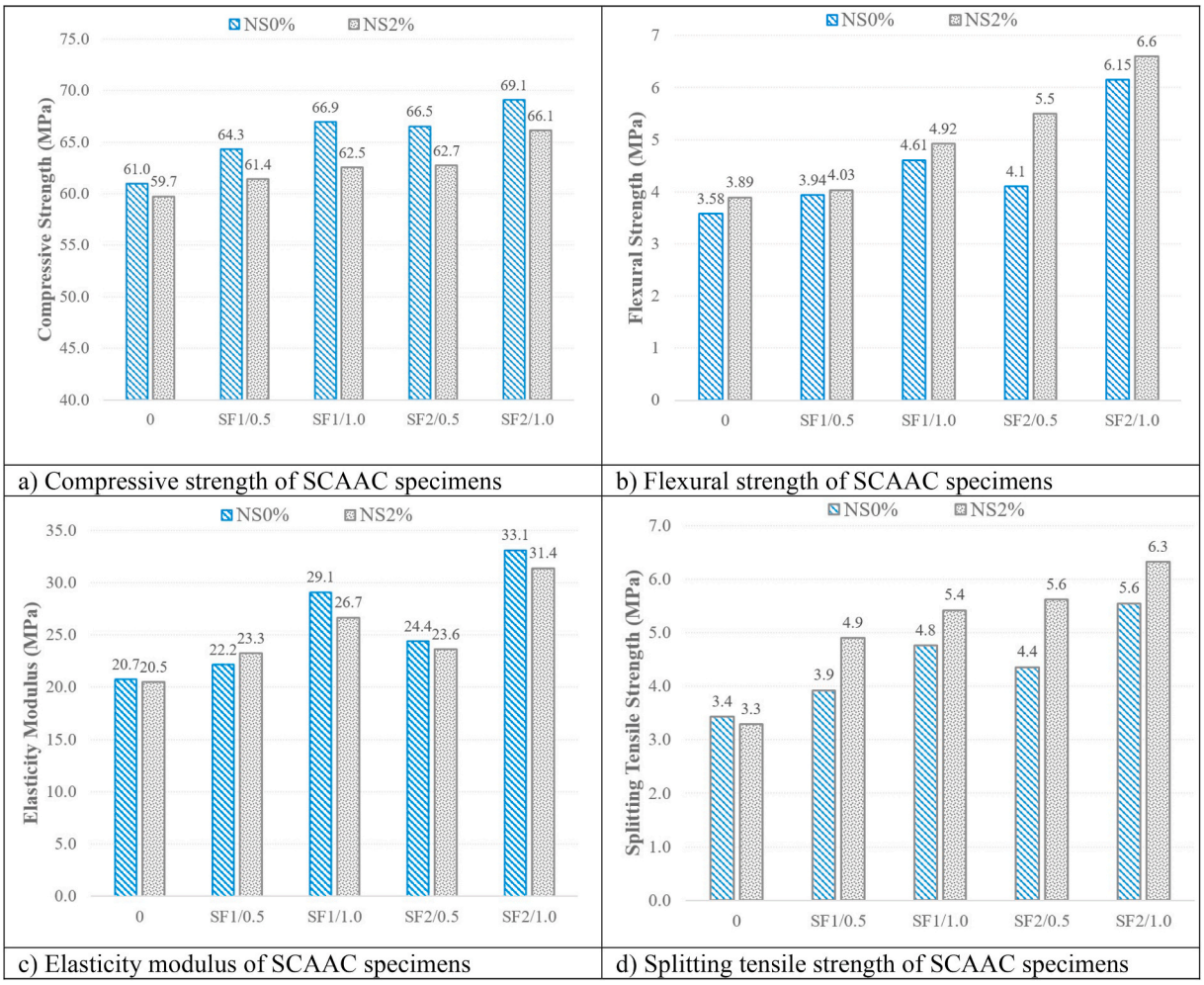

Fig. 2. The hardened state properties of SCAAC specimens.

SCC mixes had a lower flowability than 760 mm, and they were within the VF2 category. Also, slump flows of all mixes were circular, and any separation between the alkali-activated binder and aggregates was not observed. Moreover, the uniformity in the distribution of aggregates in the broken specimens showed good segregation resistance of SCC mixes. Therefore, segregation resistance was not tested in this study. However, it needs to be noted that a segregation resistance test is also required to cover SCC requirements for structural utilization.

3.2. Hardened performance of SCAAC specimens

Fig. 2 illustrates the mechanical properties of the SCAAC specimens. The results indicated that the NS incorporation had slightly decreased the compressive strength and elasticity modulus while slightly enhanced the splitting tensile and flexural strength of the specimens. Meanwhile, steel fiber inclusions enhanced all mechanical properties. The enhancement was found more with an increase in both steel fiber volume and aspect ratio, in line with other investigations [40,41]. The highest compressive strength and modulus of elasticity were obtained on GB-SF2/1.0, while the superior splitting tensile and flexural strength was reached on GBN-SF2/1.0 specimens. The higher tensile and flexural performance of specimens with 1% SF and NS can be attributed to the improved bond strength between matrix and SF resulting from the incorporation of NS [31].

3.3. Scanning electron microscopy (SEM) analysis

Fig. 3 illustrates the scanning electron microscopy (SEM) micrographs for the SCAAC samples without nanosilica (left) and with NS (right). The micrographs showed a well-distributed matrix containing less unreacted ground granulated blast furnace slag particles, implying the denser and homogeneous microstructure. However, voids and macrocracks were observed in the micrographs of Fig. 2a, 2c and 2.e, which could be due to the water evaporation, rapid setting and self-drying of slag particles, and shrinkage of the highly cross-linked C-A-S-H gel-type reaction products [42,43]. These voids and macrocracks may result in the loss of bonding between the matrix and steel fibers. The SCAAC specimens with nanosilica can be visible in the micrographs of Fig. 2b, 2d, and 2.f, and relatively fewer voids and macrocracks occurred compared to specimens without NS. The nanoparticles of NS filled the voids and cavities, and enhanced pore structure with reduced porosity was obtained. A similar SEM observation result shows that nanosilica reduces the pore amount and stimulates a toughening mechanism in the earlier investigation [44]. Another study also showed that the microstructure of the interfacial transition zone of aggregate and surrounding cement matrix was improved due to nanosilica incorporation [45]. In this study, NS particles could be seen on the micrographs at the fiber-matrix interface, improving the interfacial transition zone due to the fineness of NS, which enhanced the bonding between steel fiber and matrix. The bond strength improvement between matrix and fiber due to the nanosilica incorporation was also reported [31]. The improvement in the splitting tensile and flexural strength due to the NS addition can be

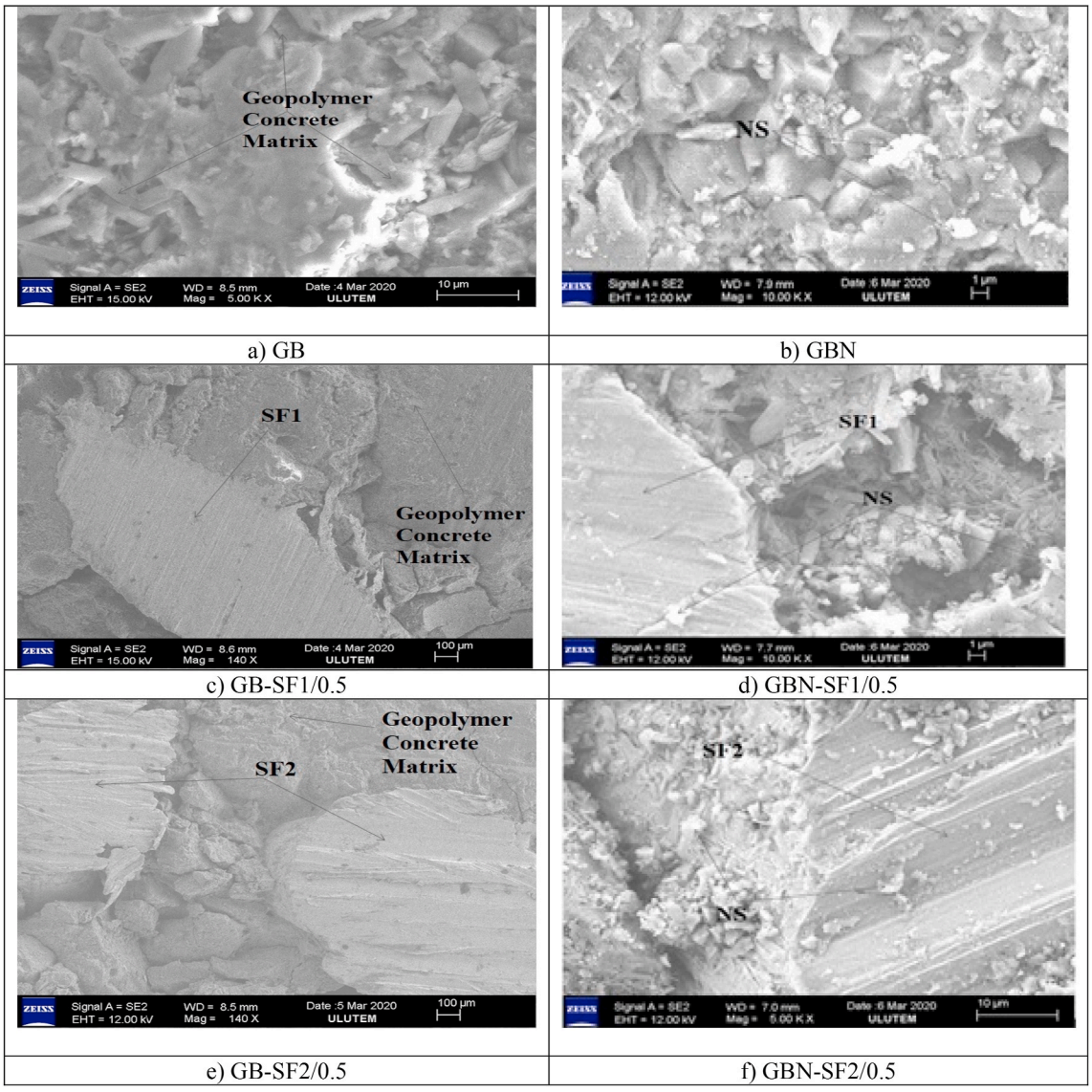

Fig. 3. SEM micrographs of SCAAC specimens with/out nanosilica.

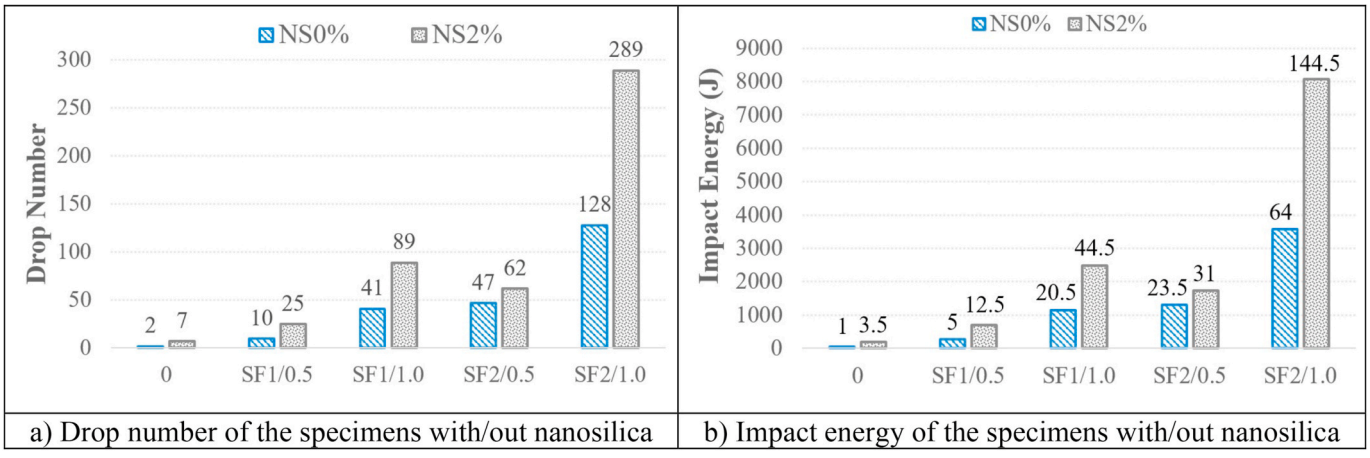

Fig. 4. Drop number and impact energy of the SCAAC specimens.

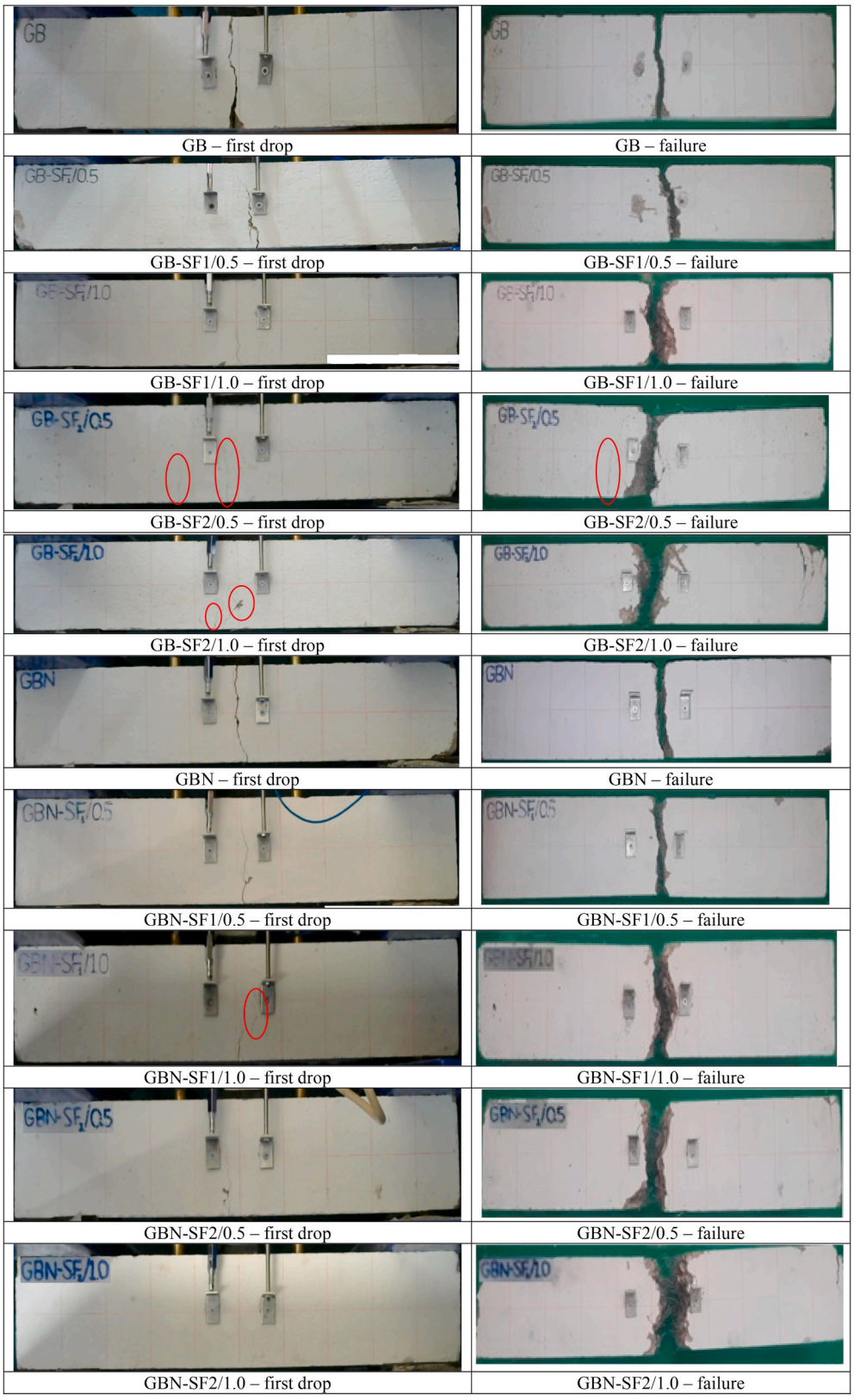

Fig. 5. The conditions of the specimens after first drop and failure.

attributed to the reduced porosity and enhanced microstructure.

3.4. Impact energy

Fig. 4. a shows the drop-weight impact test results of the beam SCAAC specimens. The number of blows required to cause ultimate failure found as 2, 10, 41, 47, 128 for GB, GB-SF1/0.5, GB-SF1/1.0, GB-SF2/0.5, GB-SF2/1.0 specimens, respectively. The impact energy, energy absorption capacity under impact loading can be the best indicator of the specimens when the impact performance of the SCAAC specimens

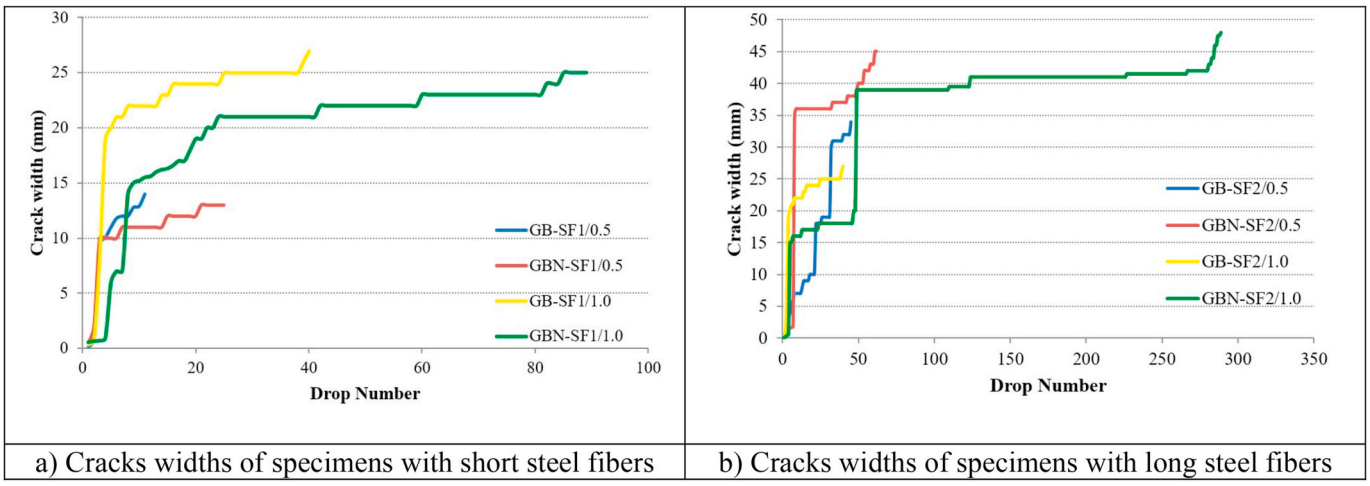

a) Cracks widths of specimens with short steel fibers b) Cracks widths of specimens with long steel fibers

Fig. 6. Crack widths of specimens under impact loadings.

is evaluated. Fig. 4.b also illustrates the impact energy comparison of the specimens with respect to GB (reference) specimen. The top values in Fig. 4.b represent the impact energy ratio of the specimens concerning GB (reference) specimens. The results pointed out that the impact energy of the specimens increased 5 times for 0.5% and 20.5 times for 1% short steel fiber (Keremix 30/40) incorporations. For the long steel fibrous (Dramix 60/80) specimens, impact energy increments were 23.5 times for 0.5% and 64 times for 1% steel fiber volumes. The obtained results revealed that the steel fiber incorporation significantly enhanced the impact energy of the SCAAC specimens. The impact energy was found more with an increase in the steel fiber volume ratio. The specimens having 1% steel fiber exhibited better impact performance than the specimens with a 0.5% steel fiber. The steel fiber type also influenced the impact energy, and the specimens with longer steel fibers (Dramix 60/80) performed better impact performance than the specimens with shorter steel fibers (Keremix 30/40). This is probably due to the more friction/adherence between steel fiber and matrix when the longer steel fibers were utilized. In an earlier investigation, steel fiber lengths (25 mm and 50 mm) and steel fiber volume ratios (0%–2%) on the impact resistance of the ordinary Portland cement concrete were investigated in detail. It was reported that long steel fibers showed better impact performance than short steel fibers, and the impact performance of the fibrous specimens increased with an increase in the steel fiber volume ratio. The long steel fibrous specimens with a 2% steel fiber volume exhibited the best impact performance [46]. Similar findings were also obtained on SCAAC specimens that the specimens having longer fibers (Dramix 60/80) with a higher steel fiber volume (1%) performed the superior impact performance in this study.

Also, nanosilica addition significantly enhanced the impact resistance of SCAAC specimens with/out steel fibers. The number of blows required to cause ultimate failure found as 7, 25, 89, 62, 289 for GBN, GBN-SF1/0.5, GBN-SF1/1.0, GBN-SF2/0.5, GBN-SF2/1.0 specimens, respectively as shown in Fig. 4.a. This impact resistance improvement can be attributed to reduced porosity [47] and increased bond strength due to nanosilica incorporation [31]. Also, the impact energy improvements due to nanosilica were 3.5 times for specimens without steel fibers, 12.5 times and 44.5 times for specimens with 0.5% and 1% short steel fiber incorporations, respectively. For the long fibrous specimens, the impact energy increments of the specimens were 31 times for 0.5% and 144.5 times for 1% steel fiber volumes, Fig. 4.b. The results pointed out that the specimens including 1% long steel fibers and 2% NS exhibited superior impact performance. The 2% nanosilica incorporation improved the impact resistance of the specimens more than 2 times as compared to specimens without nanosilica. In another study, the impact resistance of ordinary Portland cement concrete specimens with different nanosilica contents (0.5%, 1%, and 1.5%) was investigated. It was reported that the number of blows for the first crack formation was not correlated with the NS incorporation; however, the number of blows for the ultimate failure increased as the nanosilica incorporation amount increased [47]. A similar finding was also obtained in this study that nanosilica incorporations enhanced the impact performance of non-fibrous and fibrous SCAAC specimens. The lower impact performance of the specimens without nanosilica can be also attributed to the poor interfacial transition zone, which might play a role in fracture propagation directly [48].

3.5. Results of the drop-weight tests

In this research, the cracking and failure mechanism of the SCAAC specimens after the first drop and the failure were illustrated in Fig. 5. A wider big bending crack was obtained after the first impactor drop, and the failure occurred on the GB (reference) specimens at the 2nd impactor drop. When the crack formation of the SCAAC specimens was investigated, the specimens with 1% steel fibers showed very low crack width at the tension zone, and even the cracks were hardly visible. The crack width of the specimens with 2% NS and 1% long SF at the first drop was observed to be lower than the 1% long steel fibrous specimens without NS. Similarly, the GBN-SF1/1.0 specimens showed lower cracks than the GB-SF1/1.0 specimens at the first drop. The specimens with 0.5% steel fiber had wider crack widths and longer crack lengths (cracks reaches from tension to compression zone) than the specimens with 1% steel fiber, and the specimens with NS exhibited relatively lower crack widths and short crack lengths than the specimens without NS at first impactor drop.

Similarly, the crack width of the non-fibrous specimens with NS was reasonably lower than that of the specimens without NS. Meanwhile, there was no influence of the steel fiber length on the first impactor drop since similar crack width and lengths were obtained for the specimens with short and long steel fibrous specimens. When the failure of the specimens under impact loadings was compared, the specimens with 1% steel fibers exhibited more energy absorption capacity since wider crack zones were observed on these specimens. The width of the crack zone became further with an increase in both steel fiber length and steel fiber volume ratio. This tremendous impact energy enhancement is primarily attributed to the crack arresting capability of SF due to their hooked ends, creating more adherence to the matrix, enabling more stress transfer amongst SF and matrix [26]. Thus, steel fibers keep the two sides of the crack bonded. The bonding parts of the specimens become enlarged with the increase in the steel fiber lengths. In conclusion, the first crack occurrence was postponed for several impact blows. As the

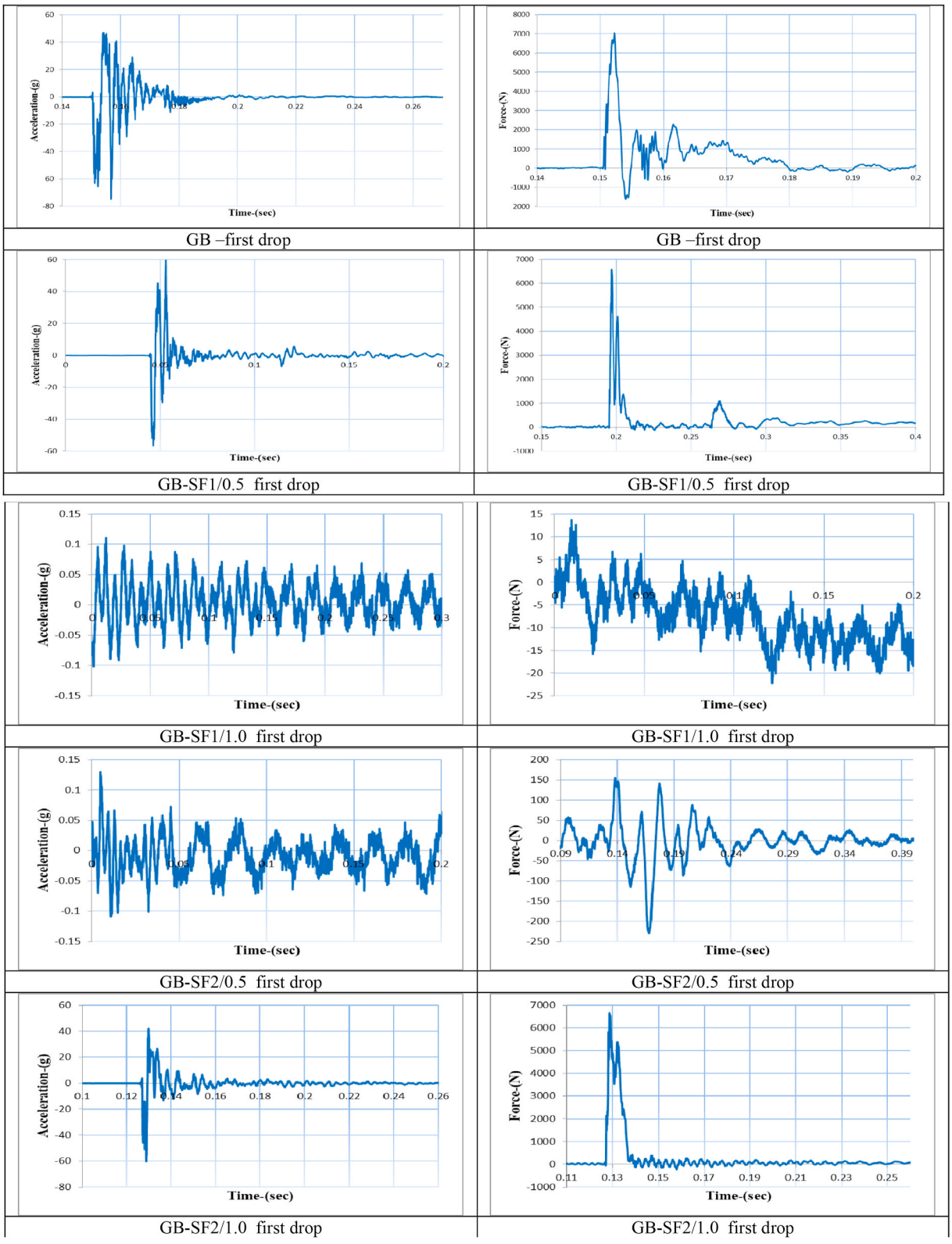

Fig. 7. Average acceleration-time and force-time graphs of the specimens for the first drop.

crack widths and lengths were increased, the tensile stress resistance of the steel fibers gets larger after each single blow, while two parts of the cracks are still bridged by steel fibers [49]. As a result, the specimen failure was delayed for several impact blows up to breaking of bond between steel fibers and matrix, where the pullout of steel fibers was the most common failure type [44,50]. Due to the higher pullout resistance resulting from higher development lengths inside the matrix, specimens with longer steel fibers showed higher impact performance than the short steel fibrous specimens. It was also noted that the higher steel fiber lengths are more efficient in reinforcing tensile, flexural, and impact

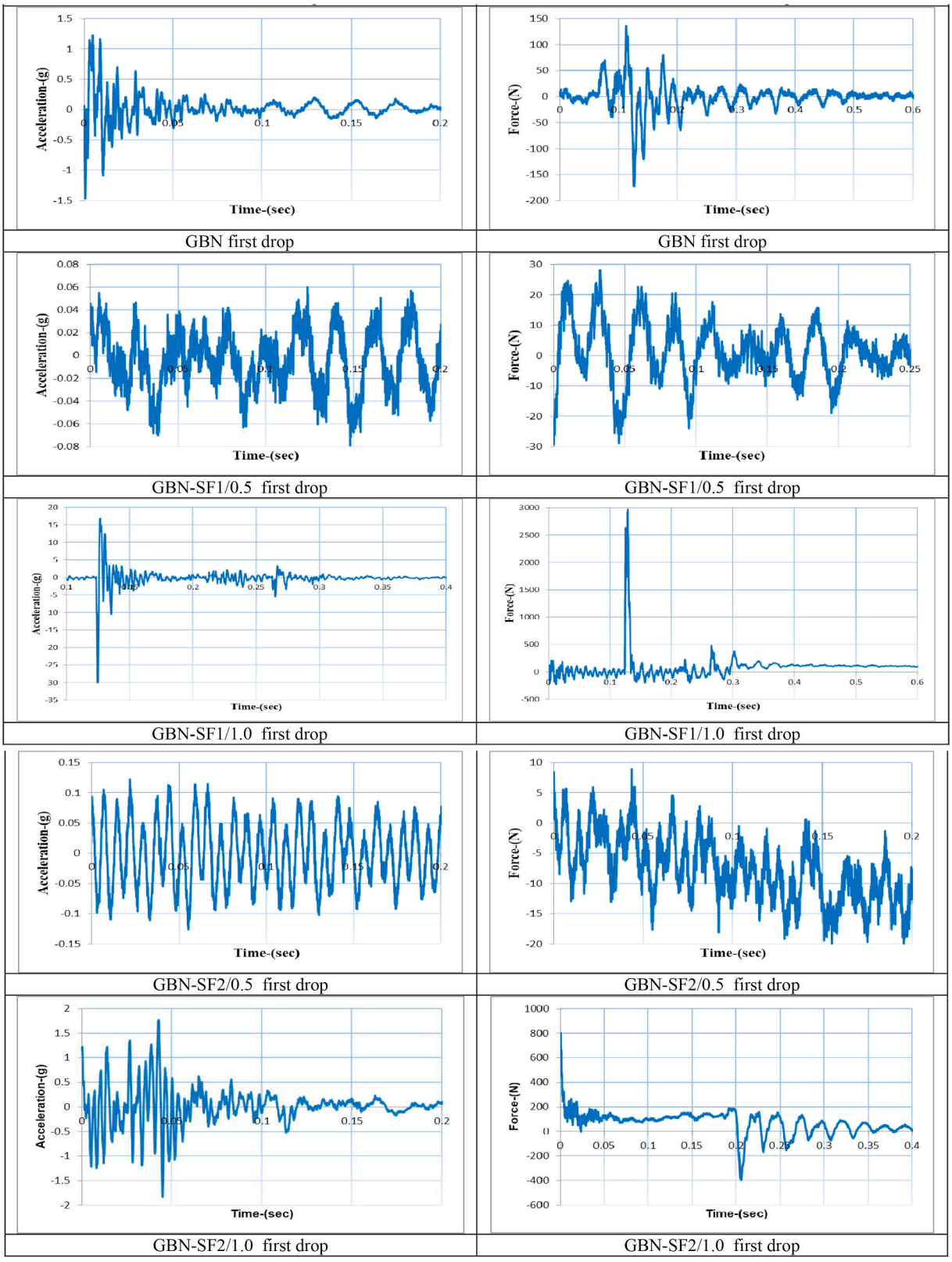

Fig. 7. (*continued*).

properties [45]. Fig. 5 also revealed that the steel fibers have the potential to prevent the crack formation and dissipate energy to the surrounding zones, and this potential increases with an increase in steel fiber length and volume ratio.

The influence of nanosilica on the impact resistance was also clearly seen on the crack width versus drop-weight number results in Fig. 6. More drop numbers were obtained for the specimens incorporating nanosilica for both specimens having SF1 (short) and SF2 (long) steel fibers. As the steel fiber volume ratio increased from 0.5% to 1%, the crack width values due to impact loadings increased, except for GB-SF2/

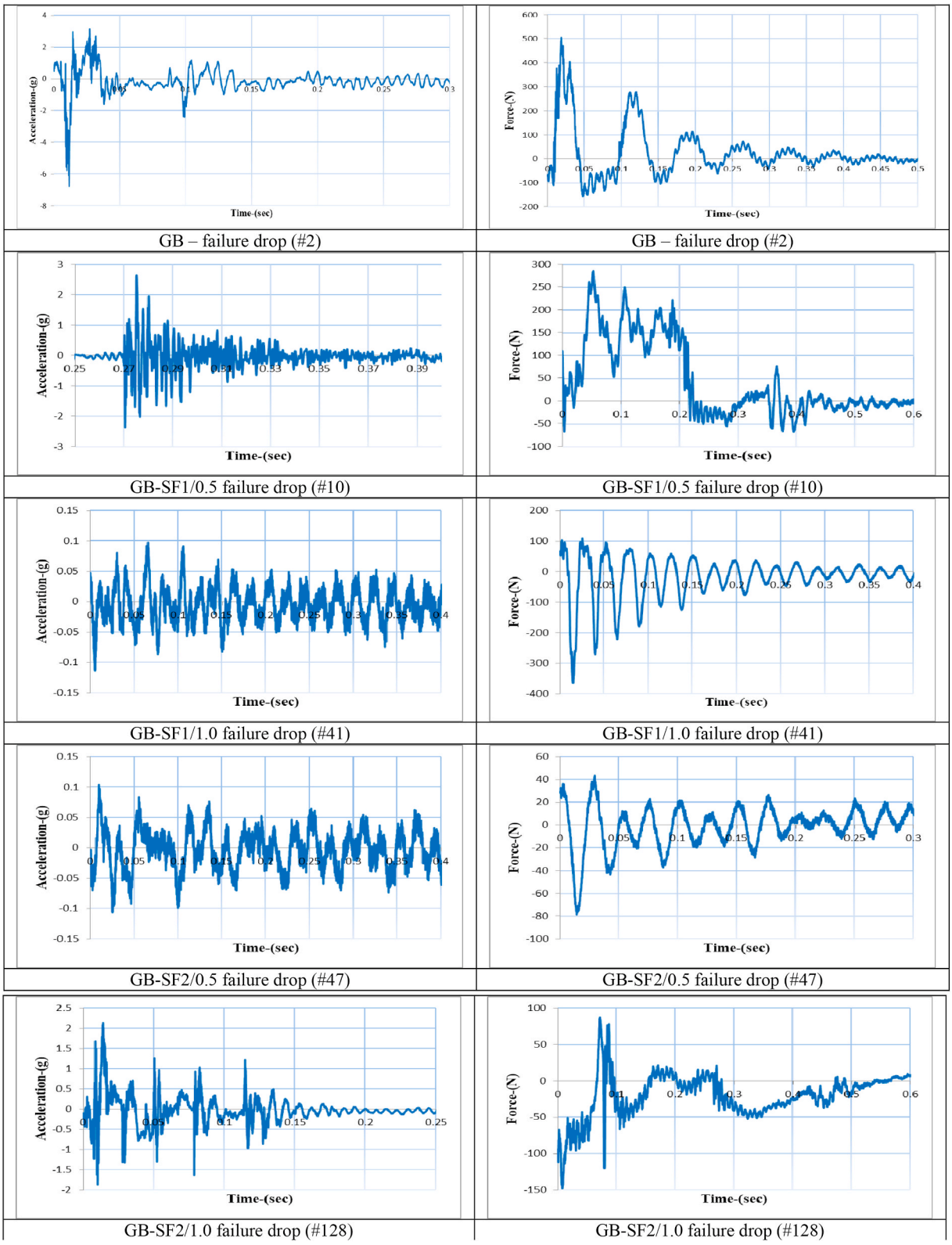

Fig. 8. Average acceleration-time and force-time graphs of the specimens for the failure drop.

1.0 specimens. More cracks were observed at the first impactor drop for GB-SF2/1.0 specimens, which reduced the width of the main responsible failure crack.

The short (SF1) and long steel fiber (SF2) lengths also influenced the final crack width values resulting from the impact loading. The specimens having longer steel fibers exhibited more crack widths than the short steel fibrous specimens, resulting in a better deformation capacity. This is probably due to the higher pullout resistance of the long steel fibrous SCAAC specimens.

Fig. 7 and Fig. 8 show the average acceleration versus time and force

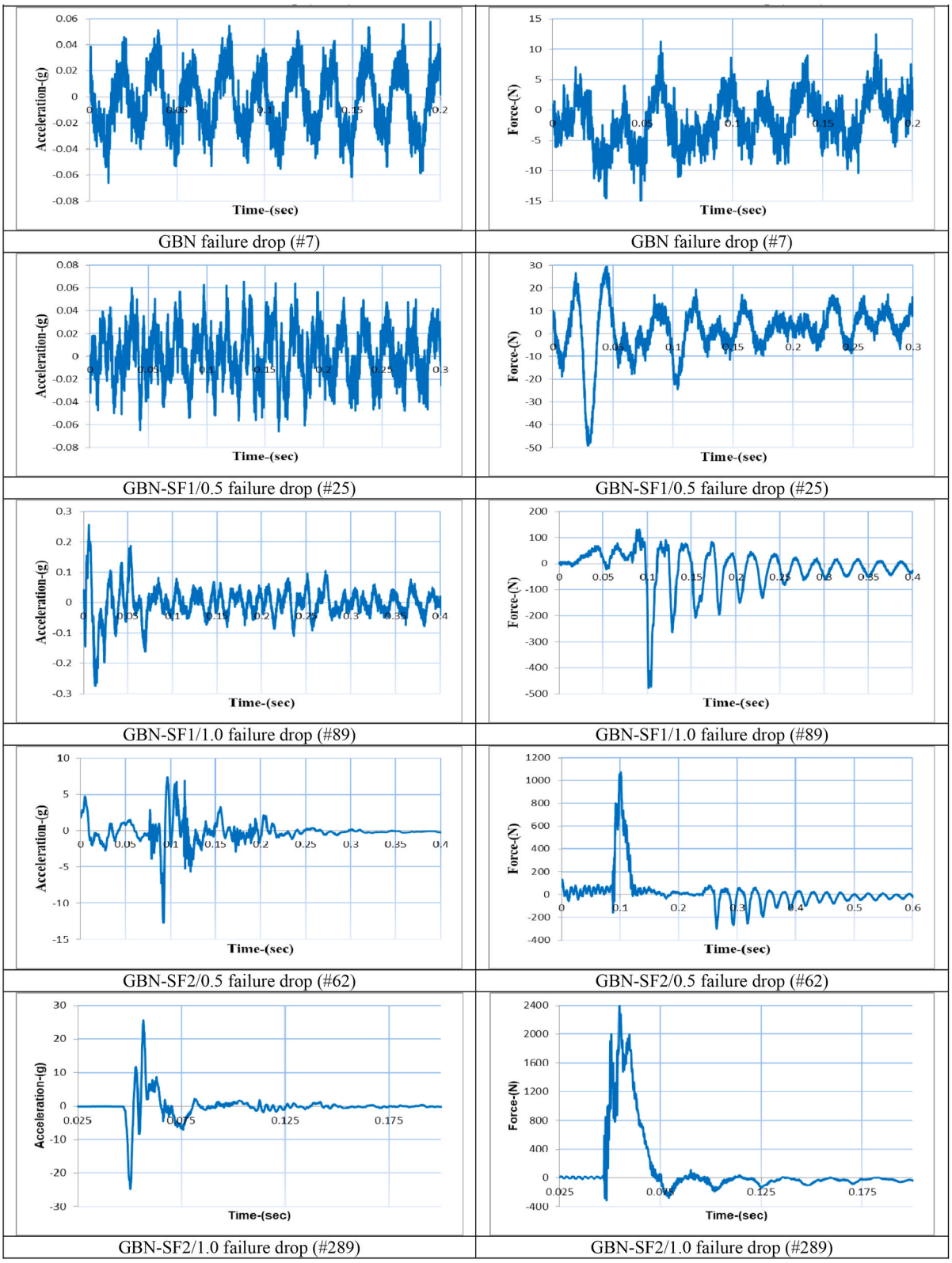

Fig. 8. (*continued*).

versus time graphs at the first drop in the case of first damage and the failure drop in the case of specimen failure (# shows failure drop number). It was reported that the average acceleration versus time result was more suitable for the impact performance evaluation than the velocity and displacements graphs, and the comments were generally based on the acceleration values from similar investigations in the literature [51]. Also, both displacement and velocity results were influenced similarly to the acceleration values in this study. Thus, the impact performance evaluations were realized using average acceleration versus time graphs. Typical acceleration versus time graphs showed that the beams start to vibrate in a similar direction to the free-fall weight. In general, the maximum acceleration results were obtained in

the first few cycles. After reaching the maximum acceleration values, beam specimens continued to vibrate with reducing amplitudes, as shown in Fig. 7 and Fig. 8. Impact load versus time graphs were also given to observe the variation of impact load with time, and the obtained results revealed that the impact loads affect the beams in a very small time interval.

The acceleration or force versus time graphs at the first drop can be evaluated together with the damage photos of the specimens, as shown in Fig. 5. The high acceleration or force values give a better indicator of the serious damage on the specimens due to the impact loading. For the GB (reference) specimens, the acceleration and force values were reached very high values, and the specimen showed a very wider crack width and crack length reaches the top fiber of the compression zone, indicating very serious damage at first drop. For the specimens with 0.5% steel fibers, cracks were reached from the tension zone to the compression zone, while cracks almost remained in the tension zone for the 1% steel fibrous specimens at first impactor drops, which is an indicator of less damage for the 1% steel fibrous specimens at first impact drops. Some of the SCAAC specimens showed more than one crack, as shown with red circles in Fig. 5, resulting in higher acceleration values and larger displacements and crack widths, which is an indicator of a high energy absorption capacity. It was noted in the earlier investigations that a rise in the acceleration values indicated the higher resistance against impact loads and higher energy absorption capacities [52], and lower acceleration values resulted in lower velocity and displacement values [51].

Some of the specimens exhibited very low impact force values for the failure drops, while others (GB-SF2/1.0, GBN-SF1/1.0, GBN-SF2/0.5, and GBN-SF2/1.0) showed higher impact force values, Fig. 7. This can be an indicator of the less impact damage up to the failure impactor drop on the GB-SF2/1.0, GBN-SF1/1.0, GBN-SF2/0.5, and GBN-SF2/1.0 specimens, which can be utilized in structural applications where higher impact energy absorption is required. A similar impact behavior finding was also explained in the earlier investigation [45]. In the study [45], the energy absorption development was divided into three stages. The first stage was called elastic collision, transferring more gravitational potential energy into kinetic energy of beams, causing lower energy absorption of the material. The second stage was attributed to the fiber pull-out process. The partially damaged beams tend to be soft due to the degeneration of stiffness, resulting in more impact energy transformation into the material deformation energy instead of kinetic energy. The last stage was a failure acceleration stage where damage degree develops faster and faster up to the overall breakage from the center occurs, and more impact energy is absorbed due to the large deformations. Similar behavior was also observed in this research on the SCAAC specimens with higher SF volumes and NS incorporating specimens.

4. Conclusions

In the research, the impact performance of slag based self-compacting alkali-activated concrete (SCAAC) with/out nanosilica and steel fibers were investigated in detail. For this aim, 2% nanosilica, short and long steel fibers with steel fiber fractions of 0.5% and 1% were utilized to investigate the influences of nanosilica and steel fibers with different lengths and volumes on the resulting impact and mechanical performances. The fresh state performance was assessed via slump flow, V-funnel, and L-box tests. The hardened state performance was evaluated using compressive strength, elasticity modulus, splitting tensile strength, flexural strength, and impact tests. The following findings were summarized below;

- The fresh state test results indicate that all SCAAC mixes had adequate flowability and passing ability based on the required limitations/standards. The additions of nanosilica slightly enhanced, while fiber incorporations decreased the flowability and passing ability. A more reduction in the flowability and passing ability was observed for the specimens having longer fibers and high fiber volumes.
- The incorporation of both nanosilica and steel fibers into slag based SCAAC adversely affects compressive strength and elasticity modulus. In contrast, they favorably affect splitting tensile strength, flexural strength, propagation of cracks, impact resistance and energy absorption capability.
- The combined utilization of nanosilica and steel fiber enhances more the splitting tensile strength and flexural strength than the individual utilization of nanosilica and steel fiber, while the combined utilization of them significantly enhanced the impact resistance and energy absorption capacity.
- The 2% NS utilization enhanced the impact resistance of SCAAC specimens with/out steel fibers more than 2 times than the specimens without nanosilica. This improvement can be attributed to the reduced porosity, enhanced microstructure, and toughening mechanism due to nanosilica.
- The incorporations of long fibers are more effective than the short fibers in increasing compressive strength, elasticity modulus, splitting tensile strength, flexural strength, impact resistance, and energy absorption capacity. The efficiency of fibers becomes more with an increase in fiber volume.
- For the specimens without nanosilica, the impact energy improvements were five times higher for 0.5% short fibrous specimens, 20.5 times higher for 1% short fibrous specimens, 23.5 times higher for 0.5% long fibrous specimens, and 64 times higher for 1% long fibrous specimens compared to the reference (without nanosilica and steel fiber) specimens. Meanwhile, for the specimens with 2% nanosilica, the impact energy improvements were 12.5 times higher for 0.5% short fibrous specimens, 44.5 times higher for 1% short fibrous specimens, 31 times higher for 0.5% long fibrous specimens, and 144.5 times higher for 1% long fibrous specimens compared to reference specimens.
- Due to the higher pullout resistance, long steel fibrous specimens showed higher crack widths than the short steel fibrous specimens, resulting in more energy absorption capacity under impact loadings. The number of blows for failure under the drop weight tests increased with both steel fiber and nanosilica incorporations. The combined utilization of nanosilica and steel fibers have the potential to delay the crack formation and dissipate energy to the surrounding zones, and this potential increased with an increase in steel fiber length and steel fiber volume ratio. The addition of nanosilica creates a strong bond between the matrix and steel fiber, which delays crack propagation.
- Average acceleration-time and force-time graphs results showed that a failure acceleration stage where damage degree develops faster and faster up to the overall failure is responsible for the failure of specimens due to the impact loadings, especially for the SCAAC specimens with nanosilica and higher steel fiber volumes. Therefore, nanosilica and steel fiber should be utilized together in structures susceptible to impact loadings such as bridges and harbors.

Declaration of competing interest

The authors declare that they have no known competing financial interests or personal relationships that could have appeared to influence the work reported in this paper.

Acknowledgement

This work was supported by Gaziantep University Scientific Research Projects Coordination Unit. Project number: MF.DT.17.06.

References

[1] R.M. Andrew, Global CO2 emissions from cement production, Earth Syst. Sci. Data 10 (1) (2018) 195–217.
[2] Z.W. Paul, N.H.A.S. Lim, M.C. Khun, A scientometric review of geopolymer concrete, J. Clean. Prod. (2020), 124353.
[3] A.E. Kurtoglu, R. Alzeebaree, O. Aljumaili, A. Nis, M.E. Gulsan, G. Humur, A. Cevik, Mechanical and durability properties of fly ash and slag based geopolymer concrete, Advances in concrete construction 6 (4) (2018) 345.
[4] R. Alzeebaree, M.E. Gulsan, A. Nis, A. Mohammedameen, A. Cevik, 'Performance of FRP confined and unconfined geopolymer concrete exposed to sulfate attacks, Steel Compos. Struct. 29 (2) (2018) 201–218.
[5] R. Alzeebaree, A. Çevik, A. Mohammedameen, A. Niş, M.E. Gülşan, Mechanical performance of FRP-confined geopolymer concrete under seawater attack, Adv. Struct. Eng. 23 (6) (2020) 1055–1073.
[6] C. Shi, B. Qu, J.L. Provis, Recent progress in low-carbon binders, Cement Concr. Res. 122 (2019) 227–250.
[7] F. Puertas, S. Martínez-Ramírez, S. Alonso, T. Vazquez, Alkali-activated fly ash/slag cements: strength behaviour and hydration products, Cement Concr. Res. 30 (10) (2000) 1625–1632.
[8] Z. Zhang, J.L. Provis, A. Reid, H. Wang, Fly ash-based geopolymers: the relationship between composition, pore structure and efflorescence, Cement Concr. Res. 64 (2014) 30–41.
[9] Y. Liu, C. Shi, Z. Zhang, N. Li, D. Shi, Mechanical and fracture properties of ultra-high performance geopolymer concrete: effects of steel fiber and silica fume, Cement Concr. Compos. 112 (2020) 103665.
[10] F.N. Okoye, J. Durgaprasad, N.B. Singh, Effect of silica fume on the mechanical properties of fly ash based-geopolymer concrete, Ceram. Int. 42 (2) (2016) 3000–3006.
[11] J. Davidovits, Geopolymers: inorganic polymeric new materials, J. Therm. Anal. Calorim. 37 (8) (1991) 1633–1656.
[12] M.N. Hadi, H. Zhang, S. Parkinson, Optimum mix design of geopolymer pastes and concretes cured in ambient condition based on compressive strength, setting time and workability, Journal of Building Engineering 23 (2019) 301–313.
[13] Y. Ma, J. Hu, G. Ye, The pore structure and permeability of alkali activated fly ash, Fuel 104 (2013) 771–780.
[14] T. Bakharev, Geopolymeric materials prepared using Class F fly ash and elevated temperature curing, Cement Concr. Res. 35 (6) (2005) 1224–1232.
[15] A. Niş, İ. Altındal, Compressive strength performance of alkali activated concretes under different curing conditions, Period. Polytech. Civ. Eng. 65 (2) (2021) 556–565.
[16] Zhang, P., Gao, Z., Wang, J., & Wang, K. Numerical modeling of rebar-matrix bond behaviors of nano-SiO2 and PVA fiber reinforced geopolymer composites. Ceramics International.
[17] A.M. Rashad, A comprehensive overview about the influence of different additives on the properties of alkali-activated slag–A guide for Civil Engineer, Construct. Build. Mater. 47 (2013) 29–55.
[18] A.M. Rashad, Effect of steel fibers on geopolymer properties–The best synopsis for civil engineer, Construct. Build. Mater. 246 (2020) 118534.
[19] S.W. Kim, S.J. Jang, D.H. Kang, K.L. Ahn, H.D. Yun, Mechanical properties and eco-efficiency of steel fiber reinforced alkali-activated slag concrete, Materials 8 (11) (2015) 7309–7321.
[20] Y. Alrefaei, J.G. Dai, Tensile behavior and microstructure of hybrid fiber ambient cured one-part engineered geopolymer composites, Construct. Build. Mater. 184 (2018) 419–431.
[21] S. Bernal, R.M. de Gutiérrez, E. Rodríguez, S. Delvasto, F. Puertas, Mechanical behaviour of steel fibre-reinforced alkali activated slag concrete, Mater. Construcción 59 (293) (2009) 53–62.
[22] S. Bernal, R. De Gutierrez, S. Delvasto, E. Rodriguez, Performance of an alkali-activated slag concrete reinforced with steel fibers, Construct. Build. Mater. 24 (2) (2010) 208–214.
[23] K. Ma, J. Feng, G. Long, Y. Xie, X. Chen, Improved mix design method of self-compacting concrete based on coarse aggregate average diameter and slump flow, Construct. Build. Mater. 143 (2017) 566–573.
[24] B.H. AbdelAleem, M.K. Ismail, A.A. Hassan, The combined effect of crumb rubber and synthetic fibers on impact resistance of self-consolidating concrete, Construct. Build. Mater. 162 (2018) 816–829.
[25] A. Nis, Mechanical properties of steel fiber reinforced self-compacting concrete, Int. J. Eng. Technol. 4 (1) (2018) 33–40.
[26] A. Niş, N. Özyurt, T. Özturan, Variation of flexural performance parameters depending on specimen size and fiber properties, J. Mater. Civ. Eng. 32 (4) (2020), 04020054.
[27] A. Çevik, R. Alzeebaree, G. Humur, A. Niş, M.E. Gülşan, Effect of nano-silica on the chemical durability and mechanical performance of fly ash based geopolymer concrete, Ceram. Int. 44 (11) (2018) 12253–12264.
[28] Y. Qing, Z. Zenan, K. Deyu, C. Rongshen, Influence of nano-SiO2 addition on properties of hardened cement paste as compared with silica fume, Construct. Build. Mater. 21 (3) (2007) 539–545.
[29] L. Senff, J.A. Labrincha, V.M. Ferreira, D. Hotza, W.L. Repette, Effect of nano-silica on rheology and fresh properties of cement pastes and mortars, Construct. Build. Mater. 23 (7) (2009) 2487–2491.
[30] M. Kooshafar, H. Madani, An investigation on the influence of nano silica morphology on the characteristics of cement composites, Journal of Building Engineering 30 (2020) 101293.
[31] M.E. Gülşan, R. Alzeebaree, A.A. Rasheed, A. Niş, A.E. Kurtoğlu, Development of fly ash/slag based self-compacting geopolymer concrete using nano-silica and steel fiber, Construct. Build. Mater. 211 (2019) 271–283.
[32] G. Yıldırım, F.E. Khiavi, Ö. Anıl, O. Şahin, M. Şahmaran, R.T. Erdem, Performance of engineered cementitious composites under drop-weight impact: effect of different mixture parameters, Struct. Concr. 21 (3) (2020) 1051–1070.
[33] N. Li, Z. Jin, G. Long, L. Chen, Q. Fu, Y. Yu, C. Xiong, Impact resistance of steel fiber-reinforced self-compacting concrete (SCC) at high strain rates, Journal of Building Engineering 38 (2021) 102212.
[34] S.R. Abid, M.L. Abdul-Hussein, N.S. Ayoob, S.H. Ali, A.L. Kadhum, Repeated drop-weight impact tests on self-compacting concrete reinforced with micro-steel fiber, Heliyon 6 (1) (2020), e03198.
[35] M. Olivia, H. Nikraz, Properties of fly ash geopolymer concrete designed by Taguchi method, Mater. Des. 36 (2012) 191–198.
[36] F.A. Memon, M.F. Nuruddin, S. Khan, N. Shafiq, T. Ayub, Effect of sodium hydroxide concentration on fresh properties and compressive strength of self-compacting geopolymer concrete, J. Eng. Sci. Technol. 8 (2013) 44–56.
[37] Z. Wu, C. Shi, W. He, L. Wu, Effects of steel fiber content and shape on mechanical properties of ultra high performance concrete, Construct. Build. Mater. 103 (2016) 8–14.
[38] M. Soutsos, A.P. Boyle, R. Vinai, A. Hadjierakleous, S.J. Barnett, Factors influencing the compressive strength of fly ash based geopolymers, Construct. Build. Mater. 110 (2016) 355–368.
[39] W. Zhang, S. Chen, Y. Liu, Effect of weight and drop height of hammer on the flexural impact performance of fiber-reinforced concrete, Construct. Build. Mater. 140 (2017) 31–35.
[40] Y. Mohammadi, S.P. Singh, S.K. Kaushik, Properties of steel fibrous concrete containing mixed fibres in fresh and hardened state, Construct. Build. Mater. 22 (5) (2008) 956–965.
[41] Ş. Yazıcı, G. İnan, V. Tabak, Effect of aspect ratio and volume fraction of steel fiber on the mechanical properties of SFRC, Construct. Build. Mater. 21 (6) (2007) 1250–1253.
[42] A. Wardhono, C. Gunasekara, D.W. Law, S. Setunge, Comparison of long term performance between alkali activated slag and fly ash geopolymer concretes, Construct. Build. Mater. 143 (2017) 272–279.
[43] N.K. Lee, J.G. Jang, H.K. Lee, Shrinkage characteristics of alkali-activated fly ash/slag paste and mortar at early ages, Cement Concr. Compos. 53 (2014) 239–248.
[44] M.P. Salaimanimagudam, C.R. Suribabu, G. Murali, S.R. Abid, Impact response of hammerhead pier fibrous concrete beams designed with topology optimization, Period. Polytech. Civ. Eng. 64 (4) (2020) 1244–1258.
[45] P.P. Li, Y.Y.Y. Cao, M.J. Sluijsmans, H.J.H. Brouwers, Q. Yu, Synergistic effect of steel fibres and coarse aggregates on impact properties of ultra-high performance fibre reinforced concrete, Cement Concr. Compos. 115 (2021) 103866.
[46] Y. Mohammadi, R. Carkon-Azad, S.P. Singh, S.K. Kaushik, Impact resistance of steel fibrous concrete containing fibres of mixed aspect ratio, Construct. Build. Mater. 23 (1) (2009) 183–189.
[47] S. Erdem, S. Hanbay, Z. Güler, Micromechanical damage analysis and engineering performance of concrete with colloidal nano-silica and demolished concrete aggregates, Construct. Build. Mater. 171 (2018) 634–642.
[48] S. Ismail, M. Ramli, Impact resistance of recycled aggregate concrete with single and hybrid fibers, MATEC Web of Conferences 47 (2016), 02001. EDP Sciences.
[49] S.R. Abid, M. Gunasekaran, S.H. Ali, A.L. Kadhum, T.S. Al-Gasham, R. Fediuk, M. Karelina, Impact performance of steel fiber-reinforced self-compacting concrete against repeated drop weight impact, Crystals 11 (2) (2021) 91.
[50] M.K. Haridharan, S. Matheswaran, G. Murali, S.R. Abid, R. Fediuk, Y.M. Amran, H. S. Abdelgader, Impact response of two-layered grouted aggregate fibrous concrete composite under falling mass impact, Construct. Build. Mater. 263 (2020) 120628.
[51] Ö. Anil, E. Kantar, M.C. Yilmaz, Low velocity impact behavior of RC slabs with different support types, Construct. Build. Mater. 93 (2015) 1078–1088.
[52] T. Yılmaz, N. Kıraç, Ö. Anil, R.T. Erdem, C. Sezer, Low-velocity impact behaviour of two way RC slab strengthening with CFRP strips, Construct. Build. Mater. 186 (2018) 1046–1063.